Tu, R., Wang, R., Ge, M., Walter, T. R., Ramatschi, M., Milkereit, C., Bindi, D., Dahm, T. (2013): Cost effective monitoring of ground motion related to earthquakes, landslides or volcanic activity by joint use of a single-frequency GPS and a MEMS accelerometer. - Geophysical Research Letters, 40, 1-5

DOI: 10.1002/grl.50653

Cost effective monitoring of ground motion related to earthquakes, landslides or volcanic activity by joint use of a single-frequency GPS and a MEMS accelerometer

R. Tu, R. Wang*, M. Ge, T.R. Walter, M. Ramatschi, C. Milkereit, D. Bindi, T. Dahm

GFZ German Research Center for Geosciences, 14473 Potsdam, Germany

Key points: (1) Joint processing of GPS and accelerometer data. (2) GPS velocity estimate using the broadcast ephemeris. (3) Monitoring of strong ground motion by combined low-cost sensors.

Abstract: Real-time detection and precise estimation of strong ground motion are crucial for the rapid assessment and early warning of geohazards such as earthquakes, landslides and volcanic activity. This challenging task can be accomplished by combining GPS and accelerometer measurements because of their complementary capabilities to resolve broadband ground motion signals. However, for implementing an operational monitoring network of such joint measurement systems, cost-effective techniques need to be developed and rigorously tested. We propose a new approach for joint processing of single-frequency GPS and MEMS-type accelerometer data in real time. To demonstrate the performance of our method, we describe the results from free-field experiments. For validations, we analyzed the dual-frequency GPS data and images recorded by a video camera through post-processing. The results of the different sensors agree very well, suggesting that real-time broadband information of ground motion can be provided by using single-frequency GPS and MEMS-type accelerometers.

Index terms: 7212, 1240, 1241, 7294, 8419

1 Introduction

Displacements associated with earthquakes and volcanic activity may span multiple scales, from sub-millimeter per year to tens of meters within seconds [Segall, 2010]. Similarly, landslides and ice sheet motions are also multi-scale. Rapid detection and quantification of this multitude of displacement scales is challenging, and commonly approached by combining various technical concepts. However, many of these displacements may involve accelerations on the order of 10^{-5} to 10 m/s^2. For technical reasons, the scales of deformation are often not fully detected, and the processes remain poorly understood.

In recent years, high-rate GPS technology has been continuously improved and increasingly useful to explore large displacements and accelerations [Bilich et al., 2008; Larson, 2009; Blewitt et al., 2009]. However, a well-known limitation of high-rate GPS is that its high precision can only be guaranteed in the low frequency band. For frequencies larger than a few hertz, the GPS data involves generally large uncertainties caused by environmental and instrumental noise [Genrich and Bock, 2006]. In comparison, digital accelerometers can measure the strong ground shaking with a much higher resolution than the GPS, but their records usually include so-called baseline errors, which are induced dominantly by ground tilting. Though these errors are generally very small, they affect seismometer records in the low frequency band and thus prevent retrieving the true ground velocity and displacement from the recorded accelerograms [Boore, 2001]. In previous studies, baseline errors of accelerometer sensors were corrected using empirical methods, which generally involve uncertainties that are not easily quantified without a geodetic reference [Wang et al., 2011].

Many approaches have suggested an integrated analysis of high-rate GPS and accelerometer data [Emore et al., 2007; Bock et al., 2011; Wang et al., 2013]. In most cases, the displacement data from a nearby GPS station is used as the reference to optimize the empirical baseline correction of the accelerometer records. To improve cost-effectiveness of co-located devices, we propose a different approach for the integrated analysis. In this approach, the site velocity is estimated using carrier phase observations of a single-frequency GPS receiver with satellite orbits and clocks from the broadcast navigation information that is decoded from the received satellite signals [Colosimo et al., 2011]. Therefore, it can be performed independently of the station and has good timeliness. In general, most of the errors can be modeled precisely [Dach et al., 2007] and atmospheric delays and biases in the satellite orbits and clocks can be significantly reduced by using epoch-differentiated observations [Colosimo et al., 2011]. However, the remaining atmospheric errors, satellite clock and orbit biases, multipath effects, and high-frequency noises are still remarkable. Such remaining errors result not only in high-frequency noises, but also a slow trend in the estimated velocity time series. According to Colosimo et al. [2011], the slow trend can be approximated to be linear for a short time period (e.g., a few minutes). For seismological observations, for example, such linear trends can be estimated through least squares regression of the data within an appropriate pre-event time window. The trend-corrected GPS velocity can then be integrated to displacement. Presently, the high-rate GPS displacement seismograms obtained in this way have an accuracy of a few centimeters [Colosimo et al., 2011].

2 Method

For cost-effectiveness, the event-trigger mode may be used to monitor strong ground motion events. In this mode, such events can be detected by using a threshold approach based on the accelerometer records, as done by a seismic early warning network [see, e.g., Fleming et al., 2009]. In practice, detection of the end of a ground motion event (such as an earthquake) is usually more complicated because of coda waves that may decay slowly but without producing any permanent ground deformation. We propose to consider that a ground motion event is over when the ground acceleration has decreased below 10% of its PGA (peak ground acceleration) for a long enough time (e.g., as long as the pre-event time window).

Once a ground motion event is detected, the joint data processing is performed in three steps. First, an appropriate pre-event time window (10-20 s) is chosen. Within the pre-event window, the ground motion is considered negligible. Thus, the initial linear trend in the GPS and the initial offset in the accelerometer baseline can be determined independently and will be removed from their respective data streams. Second, the trend-corrected GPS velocity is integrated into the GPS-based displacement, which provides the reference for the accelerometer-based displacement, so that the baseline shift in the accelerometer record can be derived by comparing the two displacement datasets. Finally, broadband ground motion information (time series of displacement, velocity and acceleration) are derived from the baseline corrected accelerometer record.

Define V_G as the real-time GPS velocity estimation based on the broadcast ephemeris and epoch-difference measurement [Colosimo et al., 2011] since an initial time $t = 0$, prior to the detected event start, denoted as t_0. Through a linear regression within the pre-event time window $[0, t_0]$, we can estimate the initial trend in V_G given by $\alpha_0 + \beta_0 t$ and extrapolate it to the whole event period. After correcting for this initial trend, we calculate the GPS-based displacement time history by integration,

$$U_G(t) = \int_0^t [V_G(\tau) - (\alpha_0 + \beta_0 \tau)] d\tau. \quad (1)$$

On the other hand, we obtain the accelerometer-based displacement time history by double integration of the accelerometer records, defined as A_S,

$$U_S(t) = \int_0^t \int_0^\tau [A_S(\xi) - A_0] d\xi \, d\tau, \quad (2)$$

where A_0 represents the pre-event baseline offset of the accelerometer sensor.

Recognizing the complementary advantage of the two measuring instruments, we may suppose that the time series $U_G(t)$ and $U_S(t)$ can be expressed in the form,

$$U_G(t) = u(t) + G_{noise}(t) \quad (3)$$

and

$$U_S(t) = u(t) + S_{trend}(t), \quad (4)$$

where u is the true ground displacement, G_{noise} represents the high-frequency noise included in the GPS-based displacement data, and S_{trend} represents the low-frequency trend in the accelerometer-based displacement data caused by the event-induced baseline errors.

Without using the GPS data, S_{trend} has to be estimated empirically. To use the GPS and accelerometer data jointly, we introduce a residual time series between U_S and U_G,

$$U_{dif}(t) = U_S(t) - U_G(t) = S_{trend}(t) - G_{noise}(t), \quad (5)$$

so that S_{trend} and G_{noise} can be estimated by the low-pass and high-pass filters applied to U_{dif}, respectively. In our approach, we determine S_{trend} by smoothing U_{dif} through a moving Gaussian window with a bandwidth of 1-2 seconds and then the true ground displacement u is calculated by subtracting S_{trend} from U_S,

$$u(t) = U_S(t) - S_{trend}(t). \quad (6)$$

As S_{trend} can be interpolated and even extrapolated for a short time, the time series u of the accelerometer sampling rate can be achieved, although the trend can only be estimated using the GPS and accelerometer data at the common epochs. The true ground velocity and acceleration are obtained by differentiating u over time.

In order to validate the low-cost combination, dual-frequency GPS and camera video data were analyzed through post-processing, as described in the next section.

3 Free-field experiment

Figure 1 shows the sledge that we used in several free-field experiments carried out in December 2012. The sledge, which can move along a table, includes a dynamic GPS antenna, a low-cost MEMS accelerometer [Fleming et al., 2009] and a high-precision accelerometer (CMG-5T Compact made by Guralp Systems Ltd). The sampling rate is 50 Hz for the GPS and 100 Hz for the two accelerometer sensors. The maximum sliding distance of the sledge was restricted to about 0.5 m in one direction. A video camera recorded the motion of the sledge from a distance of 10 m at 25 fps (frames per second). The images, with a constant pixel resolution of 3 mm, were analyzed by manual identification of the sledge and automatic image-to-image tracking using a Normalized Cross Correlation code [Walter, 2011].

We use the aforementioned joint data processing approach in simulated real-time mode for the single-frequency (L1) GPS data and accelerometer records. For illustration purposes we show a selected experiment, in which the sledge is shifted stepwise from 0 to 0.3 m. The final results of other experiment examples are summarized at the end of this section. Figure 2 shows the sledge velocity obtained from the single-frequency GPS carrier observation and the acceleration from the MEMS accelerometer records. For simplicity, the pre-event trend in the GPS velocity time series and the initial offset in the accelerometer records have been removed. To show the complementary information involved in the two different measurements, all differentiated and integrated time series are given in Fig. 2 as well.

Although the GPS velocity data and the derived acceleration seem noisy, the integrated displacements reflect an uncertainty of a few centimeters, compared with the dual-frequency GPS and camera results (Fig. 3c) as reference. In contrast, the original accelerometer-based acceleration and velocity (after the empirical baseline correction) have a much higher signal-to-noise ratio. From the post-event trend of the accelerometer-based velocity data (Fig. 2e), we can derive the permanent baseline shift of the accelerometer sensor to be 0.004 m/s^2, which can be explained by a tilt of 0.024° of the sledge after the experiment, causing the gravity to be projected in the horizontal direction (0.004 m/s^2 ≈ 9.8 m/s^2 × sin0.024°). Though this baseline shift accounts for only a few per thousandth of the peak acceleration, we observe that it is impossible to obtain the displacement through double integration of the original accelerometer record. The displacement time history shown in Fig. 2f is calculated by using the empirical baseline correction suggested by Wang et al. [2011]. This time series clearly exhibits two kinks resulting from the bi-linear approximation used for the baseline correction. Without the baseline correction, no displacement signal could be visible at all because of the large trend.

For the combined data processing, the lower sampling rate of the two measurement systems, which is 50 Hz in the present case, is used for estimating the trends. Fig. 3a shows that the residual time series U_{dif} dominates the rapid trend in the accelerometer-based displacement time series. Subtracting the smoothed U_{dif}, which we obtained by using a moving Gaussian window of 2 s (i.e., 100 epochs), from the accelerometer-based displacement U_S (black curve in Fig. 2f), we calculate the true displacement and velocity time series shown in Fig. 3b and c, respectively. Particularly, Figure 3b shows that the stepwise sliding signals of the experimental sledge have been clearly resolved with a bias less than 2-3 cm using the real-time combined data processing approach, validated by the camera (25 Hz) measurements and the results of the dual-frequency GPS obtained using the PPP approach through post-processing. In Fig. 3c, the velocity time series derived from the camera images is also shown, and the amplitude appears systematically larger than that from the low-cost combination. We explain this discrepancy by the limited pixel resolution of the camera (3 mm), leading to an overestimate of the velocity peaks. Notice that the camera-based velocity also shows stochastic noise on the same order of the overestimate.

In Fig. 4, we summarize the results from the combined data processing for the other seven free-field experiments. For each experiment, the post-event part of the combined GPS and accelerometer data is used to evaluate the uncertainty of the low-cost measurement system. In all experiments, the displacement deviations of the combined system are within 2-3 cm, using the dual-frequency GPS and camera results as reference. Note that we also tested the proposed procedure using the records by the Guralp sensor instead of the MEMS sensor, but found no substantial difference in the retrieved velocity and acceleration time series. This observation verifies the finding by Picozzi et al. [2011] that, for frequencies over 0.5 Hz, there is no significant difference between the response spectra between the MEMS and Guralp sensors that we used in this study.

4 Discussion and conclusions

We have proposed and tested a simple, but sophisticated, approach to integrate co-located high-rate GPS and accelerometer measurements. Based on our free-field experiments, the real-time accuracy of the combined system for the horizontal displacement is on the order of 2-3 cm, validated by the dual-frequency GPS and camera observations.

Note that when processing a ground motion event, the same broadcast ephemeris record has to be used during the whole event period to avoid possible jumps in the results due to the discontinuity of adjacent ephemeris records. Additionally, we emphasize that we have performed the combination of the two measurements in the displacement domain. In principle, it seems that the procedure also works in the velocity domain. However, the key achievement of the joint use is to estimate the low-frequency trend in the residual data between the accelerometer and GPS-based time series. The trend is strongly amplified through this integration and therefore can be determined more precisely in the displacement domain than in the velocity domain. Another point to be mentioned is the choice of the low-pass filter used to separate the accelerometer-based trend from the GPS-based noise. We have used the Gaussian smoothing window, which corresponds to an acausal low-pass filter because it covers the same length (1 s or 50 epochs) of past and future data. Due to the 1 s time delay, the tool that we have presented here is, strictly speaking, applicable for the near-real-time joint data processing.

In addition, the new method estimates the GPS velocity using the broadcast ephemeris received from the satellite signals directly, so that it has a better timeliness. In summary, our experimental results have shown that the combined system of a single-frequency GPS and a MEMS accelerometer is able to monitor broadband ground motion with precision satisfying most current demands in real-time seismology and earthquake engineering, with potential applications in other fields as well.

Acknowledgments

This paper is partly funded by the REAKT project (Towards Real-Time Earthquake Risk Reduction) of the European Seventh Framework Programme (Grant agreement no 282862). R. Tu is supported by the China Scholarship Council. Álvaro González and Robert A. Clements proofread the manuscript.

References

Bilich, A., J. F. Cassidy, and K. M. Larson (2008), GPS seismology: Application to the 2002 Mw 7.9 Denali Fault earthquake, *Bull. Seism. Soc. Am.*, *98,* 593-606.

Blewitt, G., W. C. Hammond, C. Kreemer, H. P. Plag, S. Stein, and E. Okal (2009), GPS for real-time earthquake source determination and tsunami warning systems, *J. Geod.*, *83,* 335-343.

Bock, Y., D. Melgar, and B. W. Crowell (2011), Real-time strong-motion broadband displacements from collocated GPS and accelerometers, *Bull. Seism. Soc. Am.*, *101,* 2,904-2,925.

Boore, D. M. (2001), Effect of baseline corrections on displacement and response spectra for several recordings of the 1999 Chi-Chi, Taiwan, earthquake, *Bull. Seism. Soc. Am.*, *91,* 1,199-1,211.

Colosimo, G., M. Crespi, and A. Mazzoni (2011), Real-time GPS seismology with a stand-alone receiver: A preliminary feasibility demonstration, *J. Geophys. Res., 116,* B11302, doi:10.1029/2010JB007941.

Dach, R., U. Hugentobler, P. Fridez, and M. Michael (2007), *Bernese GPS Software Version 5.0*, Astronomical Institute, University of Bern, Bern.

Emore, G. L., J. S. Haase, K. Choi, K. M. Larson, and A. Yamagiwa (2007), Recovering seismic displacements through combined use of 1-Hz GPS and strong-motion accelerometers, *Bull. Seism. Soc. Am., 97,* 357-378.

Fleming, K., M. Picozzi, C. Milkereit, F. Kuehnlenz, B. Lichtblau, J. Fischer, C. Zulfikar, O. Ozel, and the SAFER and EDIM working groups (2009), The Self-Organising Seismic Early Warning Information System (SOSEWIN), *Seism. Res. Lett.*, *80*, 755-771.

Genrich, J. F., and Y. Bock (2006), Instantaneous geodetic positioning with 10-50 Hz GPS measurements: Noise characteristics and implications for monitoring networks, *J. Geophys. Res., 111,* B03403, doi:10.1029/2005JB003617.

Larson, K. M. (2009), GPS seismology, *J. Geod., 83*, 227-233.

Picozzi, M., S. Parolai, M. Mucciarelli, C. Milkereit, D. Bindi, R. Ditommaso, M. Vona, M.R. Gallipoli, and J. Zschau (2011), Interferometric analysis of strong ground motion for structural health monitoring: The example of the L'Aquila, Italy, seismic sequence of 2009, *Bull. Seism. Soc. Am.*, *101*, 635-651, doi:10.1785/0120100070.

Segall, P. (2010), *Earthquake and Volcano Deformation*, Princeton University Press, Princeton and Oxford.

Walter, T. R. (2011), Low cost volcano deformation monitoring: Optical strain measurements and application to Mount St. Helens data, *Geophys. J. Int.*, *186* (2), 699-705, doi:10.1111/j.1365´-246X.2011.05051.x.

Wang, R., B. Schurr, C. Milkereit, Z. Shao, and M. Jin (2011), An improved automatic scheme for empirical baseline correction of digital strong-motion records, *Bull. Seism. Soc. Am., 101*, 2,029-2,044.

Wang, R., S. Parolai, M. Ge, M. P. Jin, T. R. Walter, and J. Zschau (2013), The 2011 Mw 9.0 Tohoku earthquake: Comparison of GPS and strong-motion data, *Bull. Seism. Soc. Am.*, doi:10.1785/0120110264.

Figure captions

Figure 1. A sketch of the experiment sledge consisting of a GPS receiver, a video camera, a low-cost accelerometer of the MEMS (SM1) and a high-precision accelerometer of the Guralp (SM2).

Figure 2. Sledge acceleration, velocity and displacement based on the single-frequency GPS (panels a-c) and MEMS accelerometer data (panels d-f). The original velocity derived from the GPS carrier observations and acceleration from the MEMS accelerometer records are plotted in (b) and (d), respectively. The bi-linear red curve in (e) represents the empirical correction of the event-induced trend in the accelerometer-based velocity time series.

Figure 3. Results from the combined processing of the GPS and accelerometer data for the selected experiment. a) Residual time series U_{dif} between the accelerometer- and GPS-based displacement time series. b) Displacement time series u retrieved by subtracting the smoothed U_{dif} from the accelerometer-based displacement, validated by the dual-frequency GPS (blue) and camera results (red). c) Velocity time series $v = du/dt$, compared with the camera observations.

Figure 4. Results from the other seven experiments. Left column: Displacement time series retrieved using the combined processing of the GPS and accelerometer data, validated by the results from the dual-frequency GPS (blue) and camera observations

(red). Middle column: Velocity time series obtained by differentiating the corresponding displacement time series. Right column: Acceleration time series given by the records of SM1.

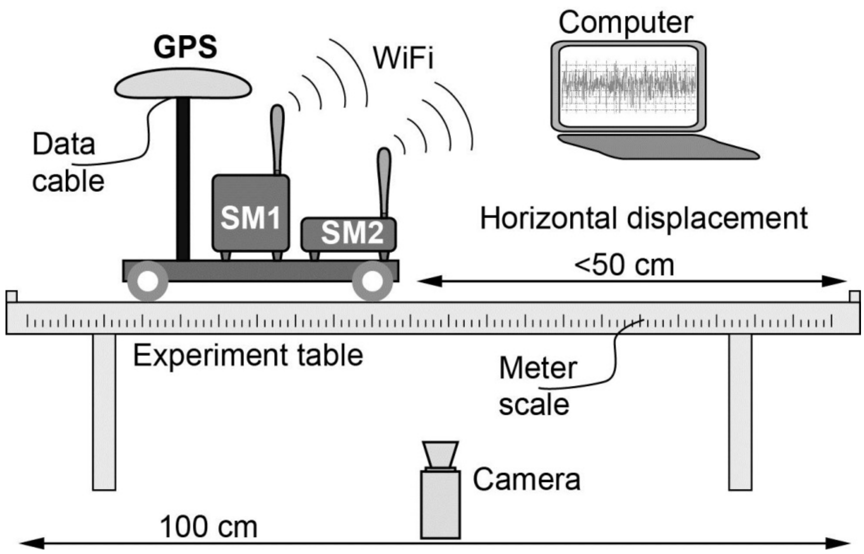
GPS
WiFi
Computer
Data
cable
SM1
SM2
Horizontal displacement
<50 cm
Experiment table
Meter
scale
Camera
100 cm

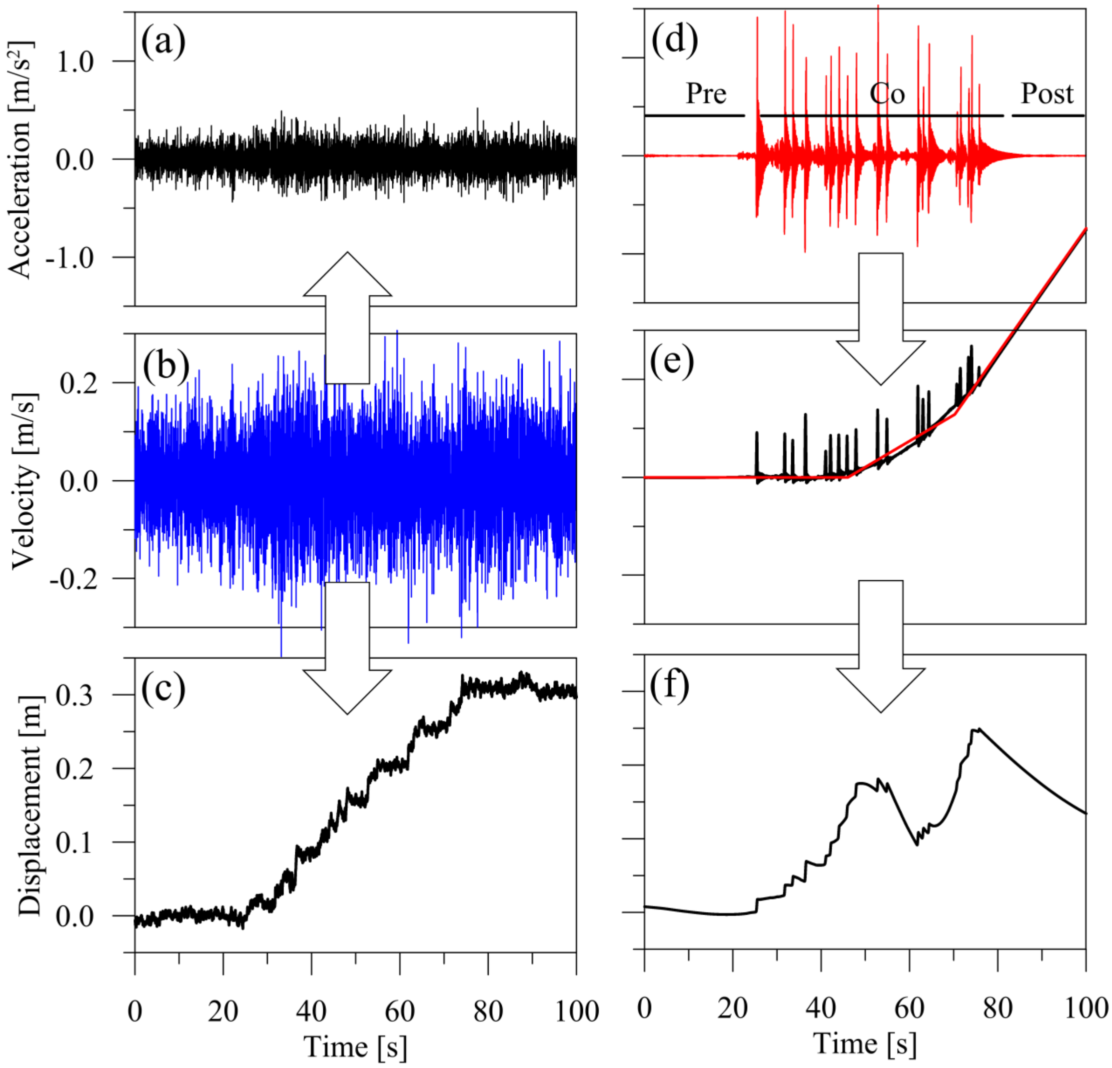

(a)
Acceleration [m/s²]
1.0
0.0
-1.0
(b)
Velocity [m/s]
0.2
0.0
-0.2
(c)
Displacement [m]
0.3
0.2
0.1
0.0
0
20
40
60
80
100
Time [s]
(d)
Pre
Co
Post
(e)
(f)
0
20
40
60
80
100
Time [s]

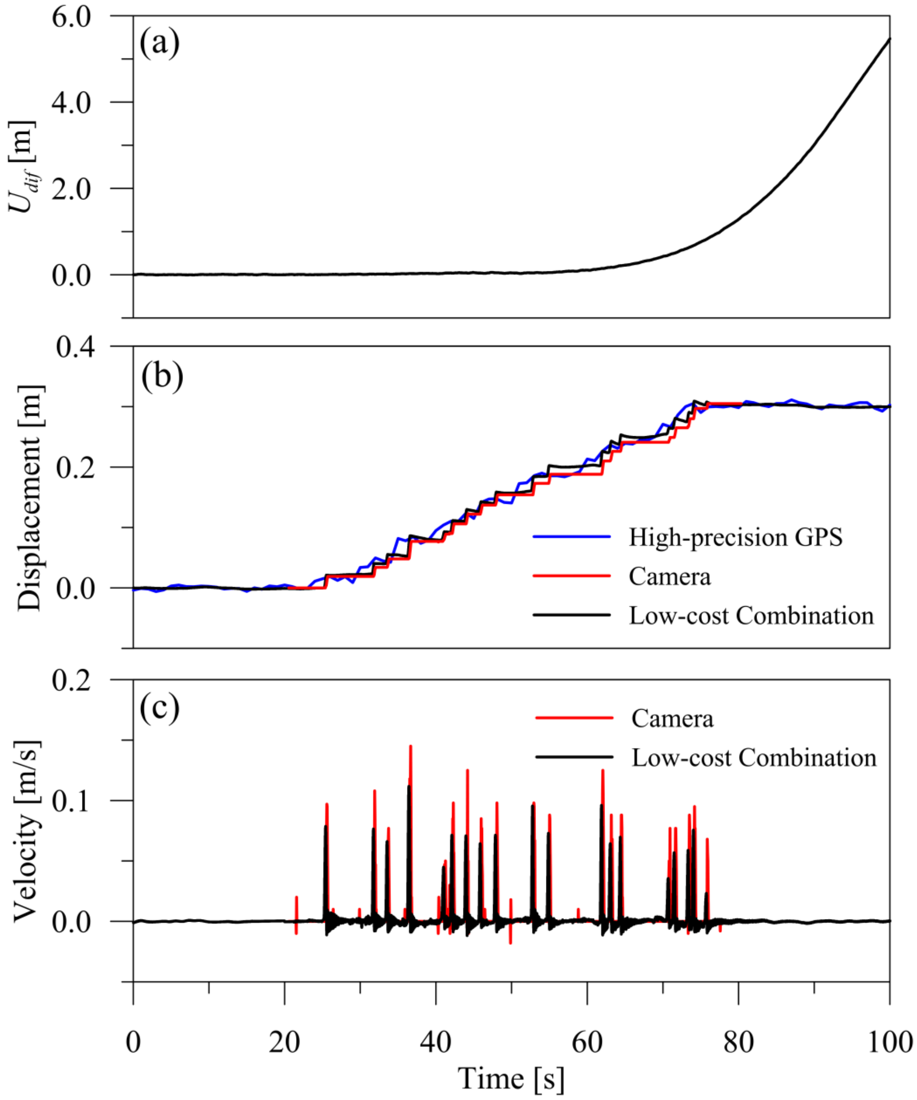

(a)
(b)
(c)
U_{dif} [m]
Displacement [m]
Velocity [m/s]
High-precision GPS
Camera
Low-cost Combination
Camera
Low-cost Combination
6.0
4.0
2.0
0.0
0.4
0.2
0.0
0.2
0.1
0.0
0
20
40
60
80
100
Time [s]

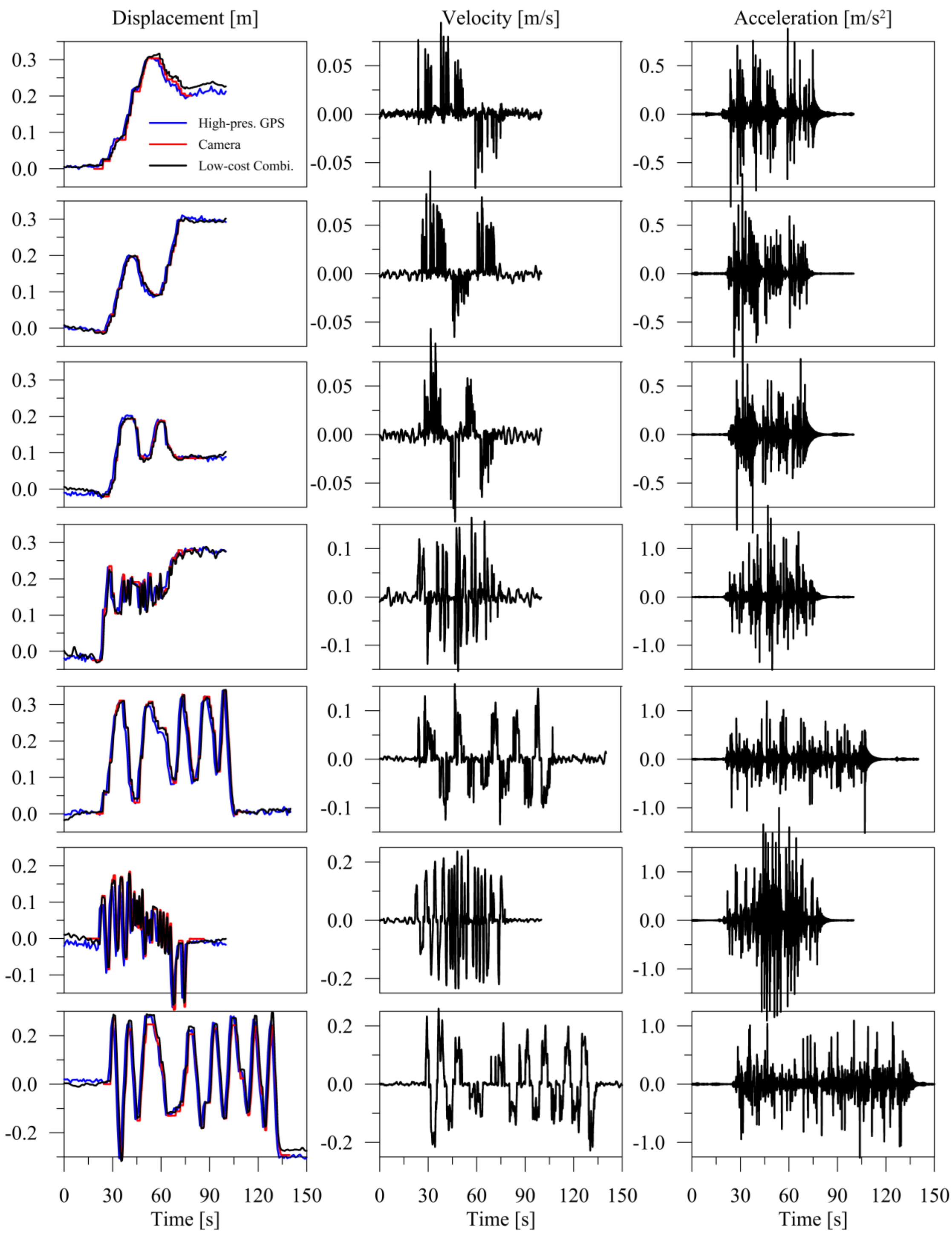

Displacement [m]
Velocity [m/s]
Acceleration [m/s²]
High-pres. GPS
Camera
Low-cost Combi.
Time [s]
Time [s]
Time [s]